RSC Advances

ROYAL SOCIETY OF CHEMISTRY

www.rsc.org/advances

Journal Name

COMMUNICATION

An active and stable Ni/Al_2O_3 nanosheet catalyst for dry reforming of CH_4

Lin Zhang and Yi Zhang *

Received 00th January 20xx,
Accepted 00th January 20xx

DOI: 10.1039/x0xx00000x

www.rsc.org/

A highly active and stable nano structured Ni/Al_2O_3 catalyst was developed by a simple two-step hydrothermal method. The obtained Ni/Al_2O_3 catalyst exhibited leaf-like nanosheet with ~5 nm thickness, and realized CH_4 conversion as high as 91.3% at 1073K with excellent stability in dry reforming of methane.

As the demand for alternative energy resources increases owing to depletion of crude oil supplies, methane has received much attention because reserves of methane are larger than that of crude oil. [1, 2] Due to both energy and environmental reasons, the reforming of methane with carbon dioxide to produce synthesis gas, CO and H_2, has received significant attention in recent years.[3-5]

Considerable research efforts have been focused on the development of active and thermodynamically stable catalysts for the CO_2 reforming of CH_4. It has been proved that supported noble metal catalysts have promising catalytic performances and low sensitivities to carbon deposition.[6–12] However, concerning the limited resources, numerous researches focused on non-noble metal catalysts. Series of research papers have reported that supported group VIII metals are good catalysts for dry reforming of methane.[13-19] A large number of publications indicate that supported nickel catalysts exhibited high catalytic activity in dry reforming of methane. The greatest problem of nickel-based catalysts is the deactivation due to carbon deposition and Ni particle sintering.

It was well reported that smaller Ni particles had a better ability to prevent coke formation.[20-23] However, for supported catalysts, the metal particles tend to aggregate during the reaction process, which leads to lower catalytic activity and coke formation.[24] Lee et al. developed highly coke-resistant Ni catalysts by coating the Ni/nano-sphere SiO_2 catalyst with silica overlayers. [2] The silica overlayer prevents the small Ni nanoparticles from sintering, and successfully suppresses the coke formation. Meanwhile, as our previously reported, [7] the highly dispersed Ni supported catalyst, prepared by modification of silica surface, realized excellent stability during dry reforming reaction, because its smaller and stable Ni particles successfully prevented carbon deposition. However, the activity of these catalysts was always damaged by coverage of Ni active sits or lower reducibility of supported nickel.

On the other hand, the hydrothermal method has been referred to as a versatile, low cost and environmentally friendly method for the preparation of catalytic materials with different size and morphology. Particles produced by hydrothermal synthesis are high purity, uniform dispersion and good crystal form. [25] However, these advantages always form abundant solid solution of active phase and support, leading to extremely strong interaction between the active metal and support, resulting in lower activity of obtained catalysts due to the poor reducibility of supported metals.

Herein, a two-step hydrothermal process was developed to synthesize the unique leaf-like nanostructured Ni/Al_2O_3 (signed as Ni/Al_2O_3 (T)) catalyst with high activity and stability in dry reforming of methane. It is believed that the $Ni(OH)_2$ nanoparticles, prepared by first-step hydrothermal process, would be partially dissolved to adjust the environment of the second hydrothermal synthesis, contributing to forming unique morphology of obtained Ni/Al_2O_3 catalyst. On the other hand, the residual $Ni(OH)_2$ nanoparticles would provide the precursors of NiO with better reducibility, which would be anchored by solid solution of dissolved $Ni(OH)_2$ nanoparticles and formed Al_2O_3, contributing to excellent thermal stability of obtained catalyst. The products were collected and purified by repeated centrifugation and then dried at 393 K for 2 h. Calcination step was carried out by slowly increasing temperature from room temperature to 773 K (2 K/min) and keeping at 773 K for 3 h. For characterization of reduced catalysts, the calcined catalysts were reduced by pure hydrogen at 1073 K for 2 h and then passivated by 1% O_2 in N_2 to form a metal oxide layer on the surface of metal particle in order to preventing oxidation of nickel metal when the catalysts were exposed to air. For comparison, another two Ni/Al_2O_3 catalysts were prepared by one-step hydrothermal (signed as Ni/Al_2O_3 (O)) and conventional impregnation method (signed as Ni/Al_2O_3 (I)).

State Key Laboratory of Organic–Inorganic Composites, Department of Chemical Engineering, Beijing University of Chemical Technology, Beijing 100029, China. Fax: 86-10-64423474; Tel: 86-10-64447274; E-mail: yizhang@mail.buct.edu.cn

† Electronic Supplementary Information (ESI) available: Experimental details, TEM images of catalyst at different stage of experiments, XRD, H_2-TPR and TG / DTA patterns of catalysts, textural and structural characteristics of the synthesized samples. See DOI: 10.1039/x0xx00000x

The morphology of the fresh catalysts was determined by Scanning Electron Microscopy (SEM). As shown in Fig. 1a, the Ni/Al_2O_3 (T) exhibited significant different morphology to other catalysts as leafy-like nanosheets (~700 nm in length, ~150 nm in width and ~5 nm in thickness). Meanwhile, the Atomic Force Microscopy (AFM) image and analysis proved the thickness of obtained Ni/Al_2O_3 (T) catalyst was in range of 4.5-5.0 nm (Figure 1e). However, large bulk was observed in SEM images of Ni/Al_2O_3 (O) and Ni/Al_2O_3 (T) catalyst, as shown in Fig 1 b and c. Furthermore,

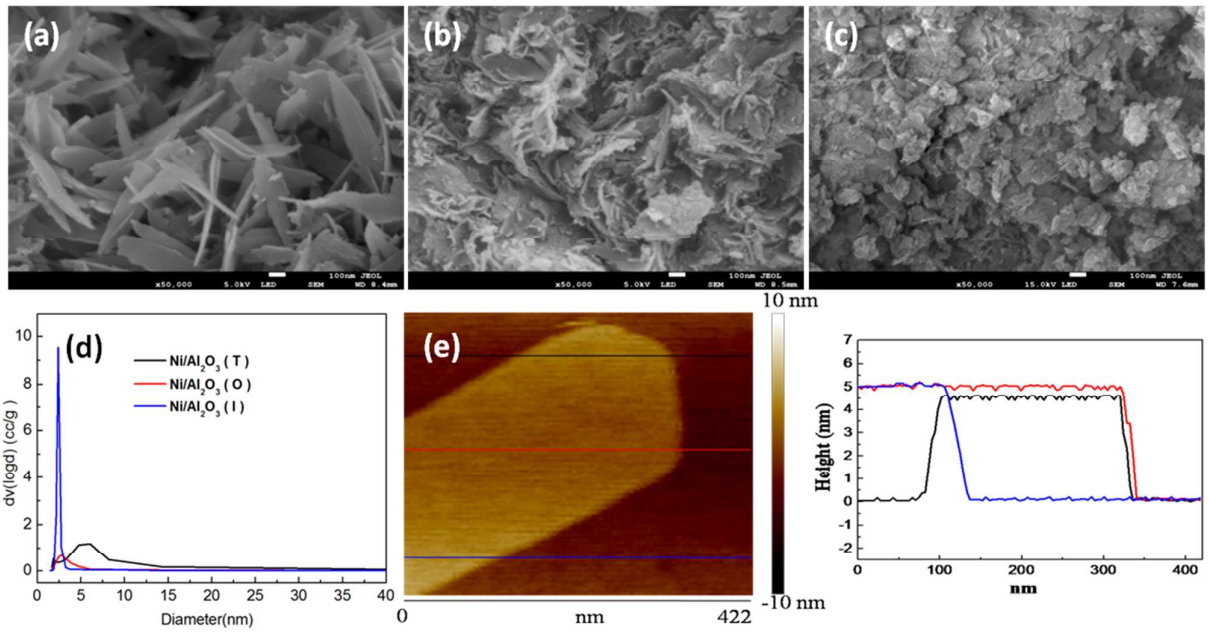

Fig.1 SEM images of the various catalysts: (a) Ni/Al_2O_3 (T), (b) Ni/Al_2O_3 (O) and (c) Ni/Al_2O_3 (I); (d) Pore distribution of obtained catalysts; (e) AFM image and analysis of Ni/Al_2O_3 (T) catalyst

the results of N_2 adsorption-desorption analysis were summarized in Table S1†. As compared in Table S1†, the BET surface area and pore volume of Ni/Al2O3 (T) catalyst was much higher than that of other two catalysts. The pore size distribution of Ni/Al_2O_3 (T) was mainly concentrated at 2.4 nm (Fig 1d and Table S1†), which was smaller than that of Ni/Al_2O_3 (O) and Ni/Al_2O_3 (I) and contributed to the larger specific surface area. It is considered that the leaf-like nanosheet structure and large pore volume would provide large channel to improve the diffusion of reactants and products, improving the activity of the Ni/Al_2O_3 (T) catalyst. Meanwhile, the large surface area would promote the dispersion of supported nickel, leading to high activity and stability. The morphology of calcined and reduced catalysts was also detected by Transmission electron microscopy (TEM) and High-resolution transmission electron microscopy (HRTEM), and the images were illustrated in Fig. 2. For the Ni/Al_2O_3 (T) catalyst, both of calcined (Fig 2a and 2b) and passivated catalyst (Fig 2 c) exhibited leaf like nanosheet structure, which is quite different to Ni/Al_2O_3 (O) and Ni/Al_2O_3 (I) catalysts. As shown in Fig 2 a (insert), clear lattice fringes with a d-spacing of 0.197 nm indexed to the [400] plane of γ-Al_2O_3, indicating that the growths of the Al_2O_3 leaves are along [400] directions.

As can be seen in Fig. 2b, the NiO particles of calcined Ni/Al_2O_3 (T) catalyst were extremely small with less than 1 nm diameter. As the precursors of NiO for Ni/Al_2O_3 (T) catalyst were $Ni(OH)_2$ nanoparticles formed by the first hydrothermal process, it is considered that during the second hydrothermal process the added $Ni(OH)_2$ nanoparticles were partially dissolved and the residual part of $Ni(OH)_2$ nanoparticles formed the extremely small NiO particles during calcination step. However, as shown in Fig. 2c, after reduction step, the homogeneous nickel metal clusters were formed with a diameter of 10 nm, which consisted of several Ni particles with 2 nm diameter. The nickel clusters of Ni/Al_2O_3 (T) catalyst were confined in specific area and effectively separated from each other, which were quite different to that of Ni/Al_2O_3 (O) and Ni/Al_2O_3 (I) catalysts. It is believed that the well confined and separated Ni clusters would prevent sintering of Ni active phase during dry reforming of methane, contributing to excellent stability of this catalyst. The morphology of metallic Ni particles of Ni/Al_2O_3 (T) catalyst was also determined by HRTEM. The nanoparticle consisted of two different crystalline, where the lattice fringes of the core crystalline was 0.203 nm, assigned to the (111) plane of the metallic Ni, and the lattice fringes around the metallic Ni was 0.24 nm, assigned to the (311) plane of $NiAl_2O_4$ (Fig. 2d). It is considered that the dissolved $Ni(OH)_2$ particles formed the $NiAl_2O_4$ to anchor the Ni metal particle formed from residual $Ni(OH)_2$ particles. Meanwhile, the dissolved part of $Ni(OH)_2$ modified the around environment of $Ni(OH)_2$ particles in second hydrothermal system leading to synthesis of leaf-like nanosheets of Al_2O_3.

The morphology of passivated Ni/Al_2O_3 (T) catalyst was also detected by Scanning Transmission Electron Microscopy (STEM). As shown in Fig. 3a, the STEM image of the catalyst exhibited similar images to Fig 2c, as leaf-like nanosheets contained the separated Ni clusters. The chemical composition of this catalyst was determined

by the energy-dispersive spectroscopy (EDS) elemental mapping analysis. As shown in Fig. 3b-d, Ni, O and Al mapping images clearly reveal chemical composition and distribution. Ni clusters consist of several nickel particles (bright green colour) and surrounded by solid solution of Ni and Al_2O_3 (light green colour).

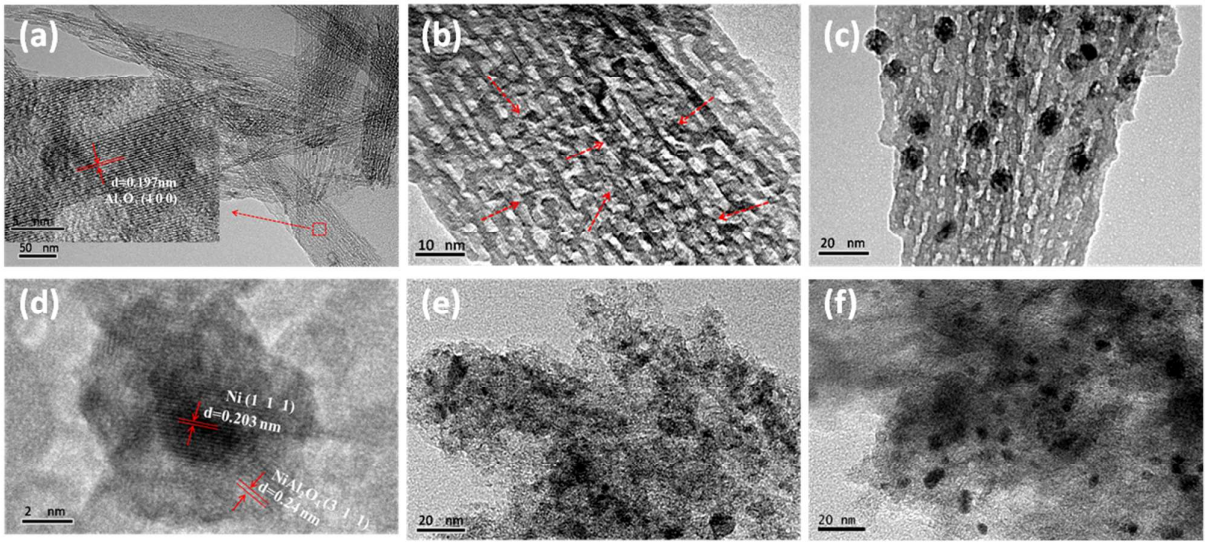

Fig.2 TEM images of various catalysts. (a and b):fresh Ni/Al_2O_3 (T), (c and d): passivated Ni/Al_2O_3 (T), (e): passivated Ni/Al_2O_3 (O), (f): passivated Ni/Al_2O_3 (I).

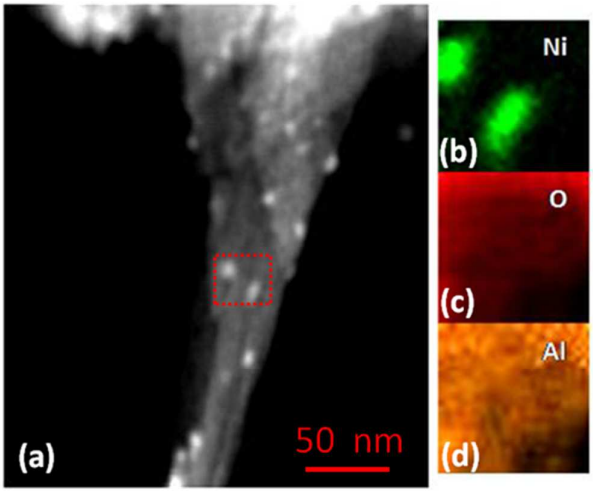

Fig.3 STEM/EDS micrographs displaying the morphologies of Ni incorporated onto the surface of Al_2O_3 after passivation. STEM image of Ni/Al2O3 (T) (a); Elemental mapping analysis: Ni (b); O (c); Al (d).

From the observed morphologies of the samples at different stages of the second hydrothermal process (Fig S1†, detailed discussion), it is believed that the $Ni(OH)_2$ particles (5nm) would partially dissolved into the solution of second hydrothermal reaction, leading to modifying the crystallization of Al_2O_3. The $Ni(OH)_2$ particles underwent a part-dissolution process in the second hydrothermal reaction and leaf-like nanosheet structure of Ni/Al_2O_3 (T) catalyst was formed via oriented attachment growth of crystals.

X-ray Diffraction (XRD) patterns of the fresh and passivated catalysts are shown in Fig. S2†. For various calcined catalysts, no diffraction peaks of NiO were observed in the XRD patterns, due to high dispersion of NiO or transformation of most NiO phase to $NiAl_2O_4$. [26] From Fig. S2b†, the metallic Ni peaks appeared in all passivated catalysts. This suggests that the $AlNiO_4$ or NiO have been reduced by hydrogen to form metallic Ni particles. No obvious difference was observed among three kinds of catalysts from patterns of fresh and passivated catalysts. Therefore, the reducibility of the catalysts is necessary to obtain information about the metal-support interaction.

H_2-Temperature Programmed Reduction (H_2-TPR) profiles of various calcined catalysts were shown in Fig. S3†. Besides a very small peak at 623K, the Ni/Al_2O_3 (I) exhibited two main reduction peaks at 788K and 1053K of. For Ni/Al_2O_3 (O), there was a big H_2 consumption peak at 1053K with two shoulders at 733K and 900K respectively. However, for Ni/Al_2O_3 (T), there are a broad peak located at 643K and two strong reduction peaks located at 923K and 1140K. According to previous literatures, [27-28] the peaks centered at different temperature can be related to different NiO species, namely free NiO phase located at low reduction temperature, fixed NiO phase and $NiAl_2O_4$ phase located at high reduction temperature. Therefore, it is believed that Ni/Al_2O_3 (T) catalyst contained the most of free NiO species and the strongest metal–support interaction in this study, due to its special preparation method and leaf-like nanosheet structure. For Ni/Al_2O_3 (O), the one-step hydrothermal process resulted in the worst reducibility in this study. As reported by references, [29-32] the free NiO species can form more active sites after reduction, stronger metal–support interaction is advantageous to better coke-resistance of the catalyst, and those would contribute to high activity and excellent stability of Ni/Al_2O_3 (T) during dry reforming of methane.

The obtained catalysts were tested in dry reforming of methane. The dry reforming of methane was carried out at 973 K under atmospheric pressure ($Ar/CH_4/CO_2$=4/48/48, where Ar is inner reference, GHSV= 21000$cm^3 \cdot g^{-1} \cdot h^{-1}$). Ni/$Al_2O_3$ (T) realized 76% CH_4

conversion (Fig 4a), which was much higher than that of Ni/Al_2O_3 (O) and very close to equilibrium conversion at 973K. The Ni/Al_2O_3 (I) exhibited 70% CH_4 conversion followed by quick deactivation. On the other hand, both Ni/Al_2O_3 (T) and Ni/Al_2O_3 (O) showed excellent stability during 10 hrs reaction. It is considered that more nickel and alumina solid solution was formed on these two catalysts due to the hydrothermal preparation method, which contributed to improving the stability of obtained catalyst. Meanwhile, because Ni/Al_2O_3 (T) contained more free NiO species, as proved by H_2-TPR, more active sits would be formed after reduction step, contributing to high CH_4 conversion. The conversion of CO_2 is similar to CH_4 conversion for three catalysts. In all cases, CH_4 conversions were lower than the corresponding CO_2 conversion, due to the reverse water-gas shift (RWGS) reaction during CH_4/CO_2 reforming reaction.[33]

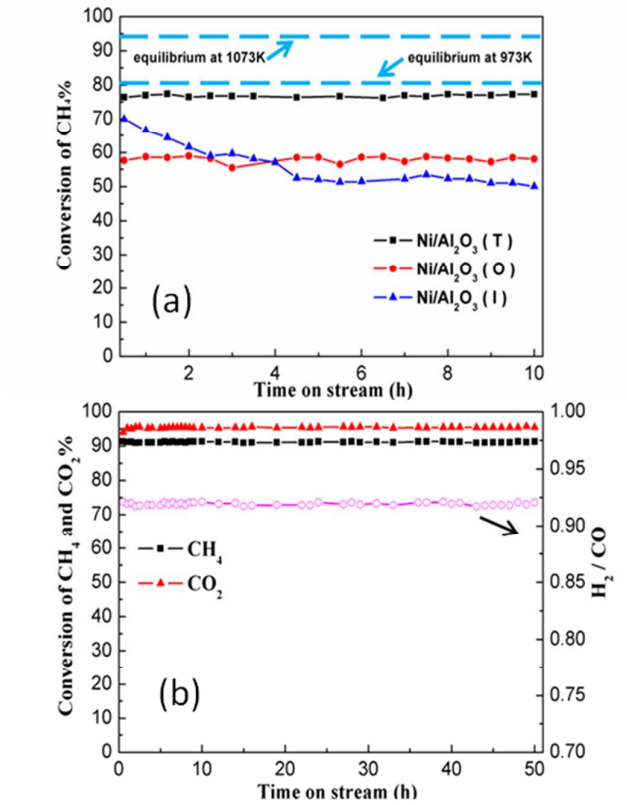

Fig.4 Reaction performance of various catalysts at 973K (a) and catalytic testing of Ni/Al_2O_3 (T) at 1073K (b). Reaction conditions: $Ar/CH_4/CO_2$=4/48/48, Catalyst: 0.1g, GHSV=21000$cm^3 \cdot g^{-1} \cdot h^{-1}$

To further investigate the stability of the Ni/Al_2O_3 (T), the CH_4/CO_2 reforming at 1073K was carried out for 50 h. As shown in Fig.4b, the ratio of H_2/CO was about 0.92 and the conversion of CH_4 reached 91.3%, which is close to the thermodynamic equilibrium conversion at 1073K (presented in Fig.4a). No decline of CH_4 conversion was observed during the whole reaction, indicating the excellent stability. The spent catalysts after 50 h reaction were characterized by TEM and TG/DTA. As shown in Fig. S4†, the TEM image of used Ni/Al_2O_3 (T), no obvious deposited carbon was found on this catalyst. Meanwhile, the TG/DTA profiles (Fig. S5†) show that the weight loss of Ni/Al_2O_3 (T) is only 5%, implying its excellent resistance of carbon deposition during the dry reforming of methane. It is believed that the novel leaf-like nanosheet structure of the Ni/Al_2O_3 (T) catalyst resulted in stable nickel particle and more active sites, contributing to remarkable reaction performance. On the other hand, the leaf-like structure could accommodate the gaseous reactants with more exposed Ni active sites than conventional supported catalysts, further contributing to the catalytic activity and stability.

The spent catalysts after 10 h reaction were characterized by several characterizations. As shown in Fig.5a, the TEM images of Ni/Al_2O_3 (T) showed that the nickel clusters consisted of several small nickel particles, dispersed on the leafy-like nanosheet substrate, and the deposited carbon was not found on this catalyst. Therefore, comparing to TEM images of the passivated catalyst (Fig. 2c), it is indicated that the Ni nanoparticles firmly immobilized in the Al_2O_3 support, effectively inhibiting the aggregation, contributing to the best stability in this study. In comparison, nickel particles on Ni/Al_2O_3 (O) and Ni/Al_2O_3 (I) obviously aggregated to large particles and deposited carbon species appeared in the TEM images (Fig. 5b and c). The XRD patterns of various used catalysts are illustrated in Fig. S6†. Compared with the XRD patterns of Ni/Al_2O_3 (T) and Ni/Al_2O_3 (O), the Ni/Al_2O_3 (I) exhibits larger metallic Ni peaks and strong diffraction peaks attributed to deposited carbon species, indicating the extremely sintering of nickel particles and more carbon deposition.

The amounts of carbon deposition of three catalysts were investigated by TG/DTA, as shown in Fig. S7†. The carbon deposition could occur on Ni-based catalysts in various forms, such as atomic carbon, amorphous carbon and graphitic carbon, which can be gasified to CO_2 in O_2 atmosphere at different temperature.[34, 35] From TG-DTA profiles (Fig. S7†), two types of carbon deposits are identified on Ni/Al_2O_3 catalyst, which correspond to the much reactive amorphous carbon at low temperature and the less reactive graphitic carbon at high temperature.[34, 35] From DTA curves (Fig S7a†), for the Ni/Al_2O_3 (I) catalyst, beside one weak exothermic peak at 608K, there was a strong peak at 903K, which indicated that numerous graphitic carbon and little amorphous carbon deposited on the Ni/Al_2O_3 (I) during activity testing. For Ni/Al_2O_3 (O), two exothermic peaks appeared at 613K and 923K were significantly weaker than those of Ni/Al_2O_3 (I), indicating that less coke deposited on Ni/Al_2O_3 (O). Furthermore, the exothermic peak of lower temperature was stronger than that of higher temperature, indicating that the active deposited carbon was more than less reactive graphic carbon, contributing to the stability of Ni/Al_2O_3 (O) catalyst. The two extremely weak exothermic peaks at 583K and 823K of Ni/Al_2O_3 (T) indicated that the much less carbon was deposited on the surface of the Ni/Al_2O_3 (T), promoting the best stability of this catalyst in this study. Generally, samples absorbed gas from the air, resulting in the weight loss before 373K. As the TG curves illustrated in Fig. S7b†, the weight loss of carbon deposition for used Ni/Al_2O_3 (T) was only 6.26%, which is much lower than that of other two catalysts (11.48% and 21.16% respectively). It is considered that the reconstitution of the firstly synthesized $Ni(OH)_2$ nanoparticles contributes to formation of highly dispersed Ni metal particles via forming solid solution around the nickel particles, which suppresses the sintering of Ni particles and leads to less carbon deposition during dry reforming of

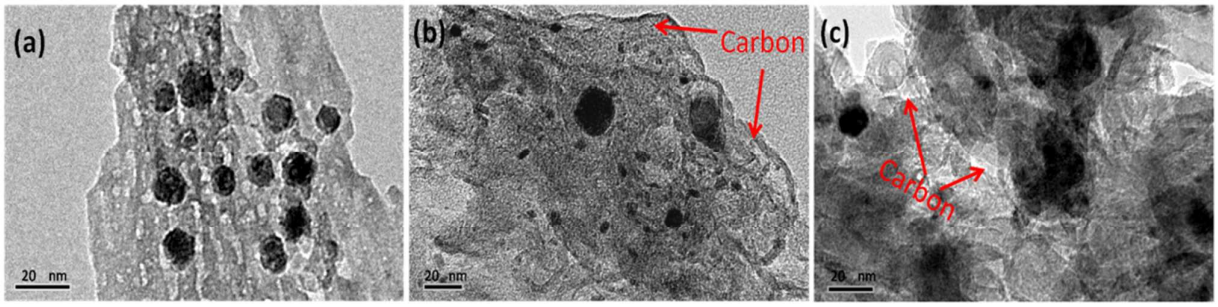

Fig.5 TEM images of used catalysts: (a) Ni/Al_2O_3 (T), (b) Ni/Al_2O_3 (O), (c) Ni/Al_2O_3 (I)

methane. Meanwhile, during the secondary hydrothermal process, the partial dissolution and re-crystallization of $Ni(OH)_2$ successfully adjusts the interaction between the supported Ni and alumina support, as proved by H_2-TPR, which might generate different interface of supported Ni and alumina support, contributing to resistance of carbon deposition. Therefore, the Ni/Al_2O_3 (T) catalyst realized extreme stability with the highest activity in this study.

Conclusions

In this work, a simple and effective two-step hydrothermal process was successfully developed to synthesize the unique leaf-like nanostructured Ni/Al_2O_3 catalyst. It is considered that the $Ni(OH)_2$ particles would partially dissolved into the solution of second hydrothermal reaction, resulting in the modified environment of the Al_2O_3 crystallization. The unique structure of Ni/Al_2O_3 (T) catalyst，the leafy-like nanosheets with ~700 nm in length, ~150 nm in width and ~5 nm in thickness, guarantees the firmly fixed active component in support and much more active sites, contributing to the highest catalytic activity and significant stability, as well as excellent resistance of carbon deposition during the dry reforming of methane. And this kind of catalyst realized 91.3% CH_4 conversion, which is close to the thermodynamic equilibrium conversion of CH_4 at 1073K, during 50 h reaction. The method demonstrated in this study, two-step hydrothermal method, offers a promising strategy for resolving the dilemma between dispersion and reducibility of supported metal, as well as activity and stability during high temperature reactions.

Acknowledgment

This work was supported by National Natural Science Foundation of P. R. China (No. 91334206, 51174259), Ministry of Education of P. R. China (NCET-13-0653), National “863” program of P. R. China (No. 2013AA031702) and Innovation and Promotion Project of Beijing University of Chemical Technology.

References

1 C. Song, *Catal. Today*, 2006, **115**, 2–32.
2 H. Lee, J. W. Han, C. Y. Kim, J. S. Park, *ChemSusChem*, 2014, **7**, 451– 456.
3 L. Tian, X. H. Zhao, B. S. Liu, W. D. Zhang, *Energy Fuels* 2009, **23**, 607–612.
4 L. Li, B. S. Liu, J. W. H. Leung, C. T. Au, A.S.-C. Cheung, *Catal. Today*, 2008, **131**, 533–540.
5 B. Steinhauer, M. R. Kasireddy, J. Radnik, A. Martin, *Appl. Catal. A*, 2009, **366**, 333–341.
6 R. Wang, H. Y. Xu, X. B. Liu, Q. J. Ge, W. Z. Li, *Appl. Catal. A*, 2006, **305**, 204–210.
7 X. Y. Lv, J. F. Chen, Y. Zhang, *Catal. Commun*., 2012, **20**, 6–11.
8 J. Z. Luo, Z. L. Yu, *J. Catal.*, 2000, **194**, 198–210.
9 E. Ruckenstein, H. Y. Wang, *J. Catal.,* 2002, **205**, 289–293.
10 X. Q. Zhang, N. Wang, Y. Xu, Y. X. Yin, *Catal. Commun.*, 2014, **45**, 11–15.
11 R. Bouarab, O. Akdim, A. Auroux, O. Cherifi, C. Mirodatos, *Appl. Catal. A,* 2004, **264**, 161–168.
12 H. Tanaka, R. Kaino, K. Okumura, T. Kizuka, Y. Nakagawa, *Appl. Catal. A,* 2010, **378**, 175–186.
13 H. Y. Wang, C. T. Au, *Appl. Catal. A*, 1997, **155**, 239-252.
14 M. C. J. Bradford, M. A. Vannice, *J. Catal.*, 1999, **183**, 69–75.
15 Michael C. J. Bradford, M. Albert Vannice, *J. Catal.*, 1998, **173**, 157–171.
16 A. Yamaguchi, E. Iglesia, *J. Catal*., 2010, **274**, 52–63.
17 S.M. Gheno, S. Damyanova, B.A. Riguetto, C.M.P. Marques, C.A.P. Leite, *J. Mol. Catal. A*, 2003, **198**, 263–275.
18 U.L Portugal, A.C.S.F Santos, S Damyanova, C.M.P Marques, J.M.C Bueno, *J. Mol. Catal. A*, 2002, **184**, 311–322.
19 A. T. Ashcroft, A. K. Cheetham, M. L. H. Green, *Nature*, 1991, **352**, 225–226.
20 Y. H. Hu, E. Ruckenstein, *Catal. Rev. Sci. Eng.* 2002, **44**, 423-453.
21 S. Tang, L. Ji, J. Lin, H.C. Zeng, K.L. Tan, K. Li, *J. Catal.*, 2000, **194**, 424–430.
22 J. Juan-Juan, M.C. Román-Martínez, M.J. Illán-Gómez, *Appl. Catal. A*, 2009, **355**, 27–32.
23 J. R. Rostrup-Nielsen, *J. Catal.*, 1984, **85**, 31–43.
24 C. Chen, C. Y. Nan, D. S. Wang, *Angew. Chem. Int. Ed.* 2011, **50**, 3725–3729.
25 X. Y. Wu , D. B. Wang, Z. S. Hu, G. H. Guet, *Mater. Chem. Phys.*, 2008, **109**, 560–564.
26 M. C. J. Bradford, M. A. Vannice, *Catal. Rev. Sci. Eng.,* 1999, **41**, 1–42.
27 Z. G. Hao, Q. S. Zhua， *Fuel process. Technol.*, 2009, **90**, 113–121.
28 J. M. Rynkowski, T. Paryjczak, M. Lenik, *Appl. Catal. A*, 1993, **106**, 73–82.
29 Y. G. Chen, K. Tomishige, K. Yokoyama, K. Fujimoto, *J. Catal.*, 1999, **184**, 179–190.
30 I. Y. Ahn, W.J. Kim, S. H. Moon, *Appl. Catal. A*, 2006, **308**, 75–81.
31 J. G. Zhang, H. Wang, A-K. Dalai, *J. Catal.*, 2007, **249**, 300–310.
32 Z. Y. Hou, T. Yashima, *Appl. Catal. A,* 2004, **261**, 205–209.

33 J. X. Chen, R. J. Wang, J. Y. Zhang, F. He, S. Han, *J. Mol. Catal. A*, 2005, **235**, 302–310.
34 A. Arenillas, S. Cuervo, A. Dominguez, J. A. Menendez, F. Rubiera, J. B. Parra, C. Merino, J. J. Pis, *Thermochim. Acta*, 2004, **256**, 99–106.
35 J. J. Guo, H. Lou, X. M. Zheng, *Carbon*, 2007, **45**, 1314–1321.

An active and stable Ni/Al_2O_3 nanosheet catalyst for dry reforming of methane

Lin Zhang and Yi Zhang *

A highly active and stable leaf-like nanosheet Ni/Al_2O_3 catalyst was developed by a simple two-step hydrothermal method.